Published in final edited form as:
Dev Biol. 2014 April 15; 388(2): 170–180. doi:10.1016/j.ydbio.2014.02.002.

Mammalian Fused is essential for sperm head shaping and periaxonemal structure formation during spermatogenesis

Yoko Inès Nozawa, **Erica Yao**, **Rhodora Gacayan**, **Shan-Mei Xu**, and **Pao-Tien Chuang***
Cardiovascular Research Institute, University of California, San Francisco, CA 94158

Abstract

During mammalian spermatogenesis, the diploid spermatogonia mature into haploid spermatozoa through a highly controlled process of mitosis, meiosis and post-meiotic morphological remodeling (spermiogenesis). Despite important progress made in this area, the molecular mechanisms underpinning this transformation are poorly understood. Our analysis of the expression and function of the putative serine-threonine kinase Fused (Fu) provides critical insight into key steps in spermatogenesis. In this report, we demonstrate that conditional inactivation of *Fu* in male germ cells results in infertility due to diminished sperm count, abnormal head shaping, decapitation and motility defects of the sperm. Interestingly, mutant flagellar axonemes are intact but exhibit altered periaxonemal structures that affect motility. These data suggest that Fu plays a central role in shaping the sperm head and controlling the organization of the periaxonemal structures in the flagellum. We show that Fu localizes to multiple tubulin-containing or microtubule-organizing structures, including the manchette and the acrosome-acroplaxome complex that are involved in spermatid head shaping. In addition, Fu interacts with the outer dense fiber protein Odf1, a major component of the periaxonemal structures in the sperm flagellum, and Kif27, which is detected in the manchette. We propose that disrupted Fu function in these structures underlies the head and flagellar defects in *Fu*-deficient sperm. Since a majority of human male infertility syndromes stem from reduced sperm motility and structural defects, uncovering Fu's role in spermiogenesis provides new insight into the causes of sterility and the biology of reproduction.

Introduction

Successful fertilization of the ovum depends on functioning sperm produced during spermatogenesis (Jan et al., 2012). The mature sperm cell (spermatozoon) is highly polarized with a nuclear head structure at one end and a flagellum at the other end to propel itself through the female reproductive tract. In the mammalian testes, the seminiferous tubules support the development of spermatogonia (undifferentiated male germ cells) into spermatozoa during spermatogenesis. This process involves mitosis of spermatogonia to produce spermatocytes, which then undergo meiosis to generate spermatids. This is followed by drastic morphological changes of spermatids, resulting in polarized spermatozoa in a highly regulated process termed spermiogenesis. Within the confines of the Sertoli nurse cells, the spermatid chromatin condenses and the nucleus elongates while the acrosome assembles on the nucleus apically to form the head structure. The acrosome cap contains

*Correspondence should be addressed to Pao-Tien Chuang: pao-tien.chuang@ucsf.edu.

hydrolytic enzymes required for penetrating the zona pellucida of the ovum. Concurrently, the basal body is anchored on the luminal side of the nucleus, from which a flagellar axoneme extends distally to form the tail. The cytoplasm shrinks and the proteins within are sorted and transported to their final destinations. Eventually, residual cytosolic components are discarded and mature spermatozoa are released from the supporting Sertoli cells (Tarulli et al., 2012) into the lumen in a process called spermiation (O'Donnell et al., 2011).

Various microtubule–based structures participate in shaping a falciform mouse spermatid head and the assembly of the flagellar tail (Sperry, 2012). Incomplete cytokinesis in mitosis and meiosis results in the formation of intercellular bridges at the site of the cleavage furrow, which allow cytoplasmic materials to be shared among hundreds of daughter cells (Greenbaum et al., 2011). Concomitantly, the spermatid chromatin condenses, a process promoted by a transient sleeve-like structure called a manchette that encases the more distal part of nucleus. It has been postulated that motor proteins on microtubule tracks of the manchette support an intraflagellar transport (IFT)-like system (called the intramanchette transport, IMT) (Kierszenbaum and Tres, 2004) to carry cargos from the nucleus to the cytoplasm and to the centrosome-derived head-tail coupling apparatus (HTCA) and the developing tail (Kierszenbaum, 2002; Kierszenbaum et al., 2011b) although direct evidence is still lacking. At the proximal end of the cell, the acrosome is anchored onto the nucleus by an F-actin and keratin-based plate called the acroplaxome (Kierszenbaum and Tres, 2004). The interaction between the juxtaposing acrosome/acroplaxome and the manchette likely contributes to head shaping through both actin– and microtubule–based transport (Kierszenbaum et al., 2003; Moreno et al., 2006). Alongside morphological changes of the head, the sperm flagellum axoneme extends distally presumably by IFT (Kierszenbaum et al., 2011b; Lo et al., 2012; Pazour et al., 2000; Zhang et al., 2013) while specialized accessory structures such as mitochondria, outer dense fibers and the fibrous sheath assemble around the axoneme (Oko and Clermont, 1989). Despite our extensive knowledge of the sequence of events during spermiogenesis, the molecular mechanisms and the players involved in this process remain poorly understood.

In previous work, we demonstrated the requirement of the conserved putative serine-threonine kinase Fused (Fu) (Stk36) in motile ciliogenesis (Nozawa et al., 2013; Wilson et al., 2009). Fu is a ciliary protein involved in constructing or maintaining the central pair apparatus of the vertebrate 9+2 axoneme in multi-ciliated tissues such as the epithelial cells of the ependyma, trachea and oviduct. As a result, *Fu* mutant cilia are dysfunctional and unable to establish directional fluid flow on the epithelial surface. An important question is whether Fu plays a similar role in the sperm flagellum that also contains the typical 9+2 microtubule arrangement in the axoneme. The early mortality of *Fu* knockout mice (Chen et al., 2005) has precluded the examination of their sperm flagellum to answer this question.

In this study, we report that conditional deletion of *Fu* in the germ cells results in male infertility and sperm motility defects. Surprisingly, *Fu*-deficient sperm flagella exhibit an intact 9+2 axoneme and instead show abnormal head shaping and defective distributions of the periaxonemal structure. Insight into Fu function comes from the observation that the Fu protein is associated with multiple organizing structures during spermiogenesis including the manchette and the acrosome-acroplaxome complex. Moreover, we demonstrate that Fu can interact with components of the manchette and the periaxonemal structures. Together, these findings establish Fu as a novel manchette-associated protein with essential roles in spermatid head shaping and tail morphogenesis.

Materials and methods

Animal husbandry and generation of transgenic mice

All mice were handled in accordance with the animal care policies of the UCSF Institutional Animal Care and Use Committee.

A conditional allele of *Fused* was previously reported (Chen et al., 2005). A *Vasa-Cre* transgenic construct (provided by Dr. Diego Castrillon) (Gallardo et al., 2007) was used to produce *Vasa-Cre* transgenic mice via pronuclear injection (Nagy et al., 2003). Transgenic mice expressing *Vasa-FuGFP* or *Vasa-Kif27GFP* were generated in a similar fashion. Mice used in this study are of mixed genetic background.

Molecular biology

Molecular cloning, genomic DNA preparation, polymerase chain reaction (PCR) and Southern analysis were performed as described (Ausubel et al., 2003; Nagy et al., 2003; Sambrook and Russell, 2001).

Fu-FLAG, Fu-3xFLAG, Fu-3xMyc, FuΔN-4xFLAG, FuΔC-4xFLAG, Vasa-FuGFP, Odf1-3xMyc, Odf1-3xFLAG, Kif27-3xMyc, Kif7-3xMyc, Vasa-Kif27GFP, Ube2b-3xFLAG and Hook1-3xMyc were constructed using standard molecular biology techniques as previously described (Wilson et al., 2009). cDNA constructs were cloned into pcDNA3 (Life Technologies) for expression in mammalian cells.

Histology and in situ hybridization

Histological analysis and section *in situ* hybridization using ^{33}P-labeled riboprobes were performed as described (Nagy et al., 2003; Wilkinson and Nieto, 1993).

Transmission electron microscopy (TEM)

Mouse testes and epididymides were fixed in 3% glutaraldehyde/1% paraformaldehyde/0.1 M sodium cacodylate, pH 7.4 at 4°C overnight and processed for electron microscopy as reported (Wilson et al., 2009).

Sperm preparations

Sperm cells were collected from adult testes and spermatozoa were harvested from the cauda epididymis as previously described (Sironen et al., 2010). Sonication-resistant nuclei of spermatids were collected using a protocol previously published (Zhou et al., 2009).

Spermatozoa motility assay

Testes and epididymides from 2-month-old male mice were dissected and weighed. Epididymal spermatozoa were squeezed out of the cauda epididymis and placed in warm human tubal fluid (HTF) medium for capacitation to occur (Luconi et al., 2005; Quinn et al., 1985). Sperm were counted for motility and progressivity using a hemacytometer. To count the total number of spermatozoa, they were placed in a 60°C bath for 3 minutes to incapacitate sperm and cooled to room temperature before counting. Alternatively, capacitated spermatozoa were filmed on a pre–warmed slide using DIC microscopy on a Nikon TE200E inverted microscope as described (Wilson et al., 2009). Individual spermatozoa were tracked using the NIH ImageJ tracker plugin or traced using Adobe Illustrator.

Immunofluorescence

Frozen and paraffin sections of mouse testes were prepared as described (Nagy et al., 2003). Dry-down slides of sperm were also used. Samples were fixed in 4% paraformaldehyde for 10 minutes, permeabilized in 0.5% Triton X-100/PBS for 15 minutes and incubated for 1–2 hours in blocking solution (3% BSA and 0.02% Triton X-100 in PBS). Standard procedures were used for immunostaining (Ausubel et al., 2003). Primary antibodies used included mouse anti-acetylated-α-tubulin (Sigma, 1:500), chick anti-GFP (Abcam, 1:500), rabbit anti-STK36 (Proteintech, 1:50) and rabbit anti-TEX14 (Abcam, 1:400). Secondary antibodies used included donkey anti-mouse Alexa Fluor 594 (Life Technologies, 1:2000), donkey anti-mouse Alexa Fluor 488 (Life Technologies, 1:2000), donkey anti-rabbit Alexa Fluor 594 (Life Technologies, 1:2000) and donkey anti-chicken Alexa Fluor 488 (Life Technologies, 1:2000).

Confocal images were acquired with a Leica TCS SPE laser scanning confocal system. Confocal stacks were collected using a 0.25 μm-0.5 μm step size along the *z*-axis. NIH ImageJ was used for image analysis.

Cell culture, transfections, Western blot analysis and immunoprecipitation

Protein expression and immunoprecipitation using anti-FLAG M2 or Myc (9E10) agarose beads (Sigma) were performed as described (Ausubel et al., 2003). Primary antibodies used included rabbit anti-FLAG (Sigma, 1:2000), rabbit anti-Myc (Sigma, 1:2000) and rabbit anti-GFP (Santa Cruz, 1:2000). Secondary antibodies used included donkey anti-rabbit HRP (Jackson ImmunoResearch, 1:4000) or IRDye 800CW goat anti-rabbit (Odyssey LI-COR Biosciences, 1:10000).

Results

Conditional inactivation of mouse Fu in germ cells results in male infertility

We previously reported that Fu is required for the construction or maintenance of the central pair apparatus in the 9+2 ciliary axoneme of multi-ciliated tissues (Nozawa et al., 2013; Wilson et al., 2009). Since the vertebrate sperm flagellum displays a similar 9+2 architecture, we asked whether Fu has a conserved role in central pair development in sperm. We first examined the expression of *Fu* and its interacting partners, kinesin *Kif27* and the central pair protein *Spag16*, in the seminiferous tubules of juvenile and adult mouse testes by *in situ* hybridization (Fig. 1A–C). Expression of all three genes in the germ cells is consistent with their potential function in spermatogenesis.

Since *Fu* knockout mice died before they reached sexual maturity, we conditionally inactivated *Fu* in the germ cells to bypass early postnatal lethality (Chen et al., 2005), thus enabling the investigation of Fu's role in spermatogenesis. To this end, we generated a *Vasa-Cre* mouse line in which the Cre recombinase was under the control of the germ cell-specific *Vasa* promoter (Gallardo et al., 2007). Using *R26R* reporter mice (Soriano, 1999), we showed that *Vasa-Cre* was expressed in germ cells (Fig. 1L). *Vasa-Cre* thus provides the necessary tool to inactivate *Fu* in germ cells and assess its function. We set up crosses to obtain *Vasa-Cre/+; Fu*$^{f/-}$ mice in which a conditional (floxed) allele of *Fu* (*Fu*^{f}) (Chen et al., 2005) was converted into a null allele (*Fu*$^{-}$) in Cre-expressing cells (*Vasa-Cre/+; Fu*$^{f/-}$ mice are designated as *Vasa-Fu* in this study). *Vasa-Fu* mice were viable and could not be distinguished from their wild-type littermates by outer appearance. The absence of *Fu* transcripts in *Vasa-Fu* testes was confirmed by *in situ* hybridization (Fig. 1F). We tested the fertility of *Vasa-Fu* males by mating and found that despite the presence of vaginal plugs in the females, the *Vasa-Fu* males failed to sire any progeny (Table 1). By contrast, loss of one allele of *Fu* in testes had no apparent effects on fertility.

Fu-deficient males have reduced mature sperm count and a large proportion of immotile sperm

Given the male infertility seen in *Vasa-Fu* mice, we were somewhat surprised to find that testes from *Vasa-Fu* and control mice were of equivalent size and exhibited comparable morphology and sperm density (Fig, 1D, I; Table 1). Not only were germ cells present in the seminiferous tubules at all stages of testes development but non-germ cells such as the interstitial Leydig and Sertoli cells were also detected in the absence of *Fu*. Likewise, histological analysis of the epididymis revealed similar morphology between *Fu*-deficient mice and controls. The head (caput) and body (corpus) of the epididymis showed no major differences in the density of (immature) sperm between wild-type and *Fu* mutants. Sperm are transferred from the testes through the caput and corpus epididymis to arrive at the tail of the epididymis (cauda epididymis). During this journey, they continue to mature. Interestingly, we noticed a slight decrease in *Vasa-Fu* sperm density in the cauda epididymis where mature sperm are stored for subsequent release (Fig. 1E, J). To confirm this finding, we sonicated the testes and cauda epididymis and isolated mature sperm heads for quantification. While only a slight reduction (~14%) in sperm count was observed in *Vasa-Fu* testes, the sperm number was reduced by ~30% in the cauda epididymis (Table 1). This result suggests a failure in sperm maturation/survival and/or elimination of defective sperm during transit from the testes into the epididymis in *Vasa-Fu* mice.

In addition to measuring sperm number, we also investigated the motility of *Vasa-Fu* sperm. Mature spermatozoa were released from the cauda epididymis, placed in warm capacitating medium (human tubal fluid solution, HTF) and tracked by video microscopy. Capacitation is a maturation step that normally occurs in the female reproductive tract in order to achieve successful fertilization (Fraser, 1998; Suarez, 2008). Upon capacitation, wild-type spermatozoa increase the amplitude of the flagellar bend, which is accompanied by waveform changes from symmetrical to asymmetrical. This could overcome the viscous environment of the oviduct and aid progression up the oviduct. The waveform is initiated as a bend at the flagellum base and is propagated along its length (Inaba, 2011). ~51% of capacitated *Vasa-Fu* spermatozoa had no motility at all (Table 2). Only ~23% of capacitated *Vasa-Fu* spermatozoa displayed progressive movement. The remaining spermatozoa (~26%) were motile; they were able to generate a bend in the flagellum under capacitation but were incapable of propagating the wave (supplementary material Fig. S1). The flagellum appeared to be constrained and failed to progress. This indicates that although these spermatozoa responded to Ca^{2+} influx in the capacitation medium and initiated a bend at the flagellum base, the signal was either too weak to propagate or was blocked by some physical hindrance within the flagellum. The absence of *Fu* severely disrupts the motility of mature sperm.

Vasa-Fu sperm exhibit abnormal head morphology and frequent decapitation

To further investigate the cause of sperm immotility in *Vasa-Fu* males, we performed a thorough morphological analysis of mature sperm collected from the caudal epididymis. Over 36% of $Fu^{-/-}$ sperm were decapitated (Table 2). Sperm that retained their heads appeared grossly normal with a flagellum of regular length. However, a closer examination revealed an unusual club-shaped morphology in nearly all *Vasa-Fu* sperm heads (Fig. 2D, E) unlike the characteristic hook shape observed in wild-type sperm heads (Fig. 2A, B). The mouse sperm heads that contain nucleic content became excessively elongated in the absence of *Fu* (Fig. 2E). Transmission electron microscopy (TEM) analysis confirmed the presence of a deformed sperm head structure in *Fu* mutants. In wild-type sperm, the acrosome cap that covers the anterior portion of the head is tightly associated with the nucleus through the acrosome-acroplaxome complex (Fig. 2C). By contrast, a large gap was detected between the acrosome and the nucleus in *Vasa-Fu* sperm (Fig. 2F). Moreover,

alteration in the shape of the nucleus, fragmentation of the membrane and excessive elongation of the manchette were observed in elongating *Vasa-Fu* spermatids (Fig. 2O–V compared with 2G–N; supplementary material Fig. S2). Deformation of the head structure may contribute to the infertility of *Vasa-Fu* males since the acrosome cap required for fertilization may not function properly. A combination of a reduced sperm count, impaired motility and structural abnormalities of the sperm head would prevent successful fertilization by *Vasa-Fu* males under normal physiological conditions.

Abnormal sperm head structure in the absence of Fu is associated with perturbed manchette structure in elongating spermatids

We speculate that an abnormal sperm head in *Fu* mutants originates during spermiogenesis. To test this idea, we followed the development of spermatids in *Vasa-Fu* male mice. Germ cells at various stages of development were dissociated from the testes, spread onto slides and probed with antibodies against the microtubules (*e.g.*, acetylated tubulin) and nuclear-staining dye DAPI. In particular, we closely monitored the appearance, maturation and disappearance of the transient manchette structure during spermiogenesis in order to uncover the molecular basis of sperm head defects in *Vasa-Fu* sperm. This is based on the observation that the emergence of a microtubule-based manchette structure around the nucleus coincides with several critical events such as the condensation of the nuclear head and protein shuttling to the developing flagellum.

We found that early round spermatids (steps 1–7) had normal morphology in *Vasa-Fu* testes. Abnormal elongation of the nuclei became visible from step 8 onward (Fig. 2E’, I’ compared with 2W, A’) and continued throughout the subsequent process of condensation and spermiation. During spermatid head development, wild-type spermatids produced a conical-shaped manchette surrounding the more distal part of the nucleus at steps 9–12 (Fig. 2X, Y, B’, C’). By contrast, the manchette in *Vasa-Fu* spermatids was elongated (Fig. 2F’, G’, J’, K’). Throughout the elongation phase of the spermatid (steps 9–12), the *Vasa-Fu* manchette was ectopically present near the proximal end of the nuclei (Fig. 2F’, G’, J’, K’). In addition, the *Vasa-Fu* manchette displayed a pincer-like appearance, and the nucleus encompassed by the manchette was elongated and narrowed compared to wild-type. These events could underlie the club-shaped nucleus of mutant spermatids. In the late spermiogenesis stages, tubulin staining was mostly restricted to the base of the head and the axoneme of the flagellum (Fig. 2Z). In *Fu*-deficient spermatids, however, a sliver of tubulin staining persisted on one side of the nucleus (Fig. 2H’), which eventually disappears in the mature sperm. The close association between abnormal manchette structure and sperm head morphology suggests that aberrant nuclear head shaping in *Fu* mutants could be caused by defective manchette function.

Vasa-Fu flagellar axonemes exhibit periaxonemal defects but retain the central pair apparatus

Impaired sperm motility in the absence of *Fu* prompted us to examine the ultrastructure of flagellar axonemes (Fig. 3A–F). In particular, we surmised the central pair apparatus is absent in *Fu* mutant sperm since loss of *Fu* is associated with central pair defects of motile cilia in all multi-ciliated tissues examined (Nozawa et al., 2013; Wilson et al., 2009). Transmission EM analysis was performed on cross-sections of epididymal and testicular sperm flagella. To our surprise, the central pair microtubules were present through the mid- and principal pieces of *Fu*-deficient flagella in both testes (Fig. 3G–L) and epididymides (supplementary material Fig. S3). The characteristic 9+2 axonemal structure remains intact in the absence of *Fu*.

We inspected other potential ultrastructural defects that could cause sperm motility defects in *Fu* mutants and uncovered abnormality in the periaxonemal structure. In the principal piece of flagellum, the axoneme and outer dense fibers are surrounded by a fibrous sheath, a cytoskeletal structure not present in cilia (Fig. 3S). The fibrous sheath consists of two longitudinal columns connected by semicircumferential ribs. Importantly, the fibrous sheath is proposed to influence the plane and shape of the flagellar bend and the flexibility of the tail (Eddy et al., 2003). We found that in *Vasa-Fu* spermatozoa, the fibrous sheath was often punctured and grossly distorted with large visible gaps within the principal piece (Fig. 3H–I). Furthermore, while the normal 8+3 positioning of the longitudinal columns was maintained in all *Vasa-Fu* flagella, one or two additional longitudinal columns were present at random positions in over 57% of the principal piece analyzed (Fig. 3O–R compared to 3M–N; supplementary material Fig. S3; Table 2). Two extra longitudinal columns (Fig. 3R) could be detected in approximately 5% of sections. The location of the additional columns in *Vasa-Fu* mice varied from animal to animal. Additional longitudinal column(s) was accompanied by the emergence of a longitudinal column anchor (LC-A) between the extra column and its corresponding doublet (Fig. 3O–R). Other periaxonemal structures such as the outer dense fibers, appeared to be unaffected in *Fu* mutants but potential mitochondrial distortion may exist (Fig. 3G). Our results suggest that the inability of the *Vasa-Fu* flagellum to initiate or maintain a propagating wave could be attributed to disruption of the fibrous sheath and the presence of additional longitudinal column(s) that would restrict the bending of the flagellum along its length and impede directional movement.

Fu is present in the manchette and the acrosome-acroplaxome complex of the developing spermatid

To further explore the molecular mechanisms by which Fu controls spermatogenesis, we assessed the subcellular distribution of Fu in the developing sperm. To this end, a transgenic mouse line was created in which the germ cell-specific *Vasa* promoter directed the expression of a Fu-GFP fusion protein (this mouse line is denoted as *Vasa-FuGFP*). Testes from *Vasa-FuGFP* were harvested at postnatal (p) day 21 and p40–100. In addition, cells were also released from the seminiferous tubules of testes for immunofluorescence analysis. We discovered that the GFP signal was detected in the cytoplasm of both immature and developing spermatocytes but not in Sertoli or other interstitial cells (supplementary material Fig. S4). Strong GFP signals appeared in the cytoplasm of spermatocytes (Fig. 4I) and early spermatids (Fig. 4A). Interestingly, at the round spermatid stage (steps 1–7) [see legend of supplementary material Fig. S5] specific signals were detected in multiple rings on the plasma membrane (Fig. 4A, E). Judging by their positions on the surface and appearance, these rings correspond to stable intercellular bridges, which connect the cytoplasm of multiple spermatids and are identified by markers such as TEX14 (Greenbaum et al., 2006) (supplementary material Fig. S6). The intercellular bridges were present through the elongation phase (steps 9–12) (Fig. 4B, C) and eventually disappeared when spermatids were fully elongated (Fig. 4D). In addition to Fu localization to the intercellular bridges, we noticed specific GFP signals in several structures associated with the appearance of the manchette. GFP signal was present on the microtubule tracks of the manchette (Fig. 4B, C, F, G, M) and the perinuclear ring of the manchette (Fig. 4M) from which microtubules radiate. Furthermore, GFP staining was observed at the proximal end of the nucleus where the acrosome-acroplaxome complex resides (Fig. 4B, C, F, G, J–L). GFP intensity dropped abruptly once the spermatid had been elongated (Fig. 4D, H). Spermiating cells only had faint cytoplasmic Fu staining in the residual bodies, which disappeared completely once sperm matured.

To confirm the localization of Fu-GFP protein in the developing spermatids, we employed a commercial antibody against STK36 (Fu) to try to detect endogenous Fu.

Immunofluorescence was observed in the acrosome-acroplaxome complex, the perinuclear ring of the manchette and the manchette (Fig. 4R, S, V, W; supplementary material Fig. S5). Importantly, the specific staining of STK36 antibodies in these subcellular structures disappeared in *Vasa-Fu* germ cells (Fig. 4Y-B'; supplementary material Fig. S5). This provides strong evidence to suggest that transgenic FuGFP signals in spermatids largely recapitulate the endogenous Fu expression patterns. The intensity is different between FuGFP and STK36 in various subcellular locales likely due to overexpression of FuGFP. We conclude that Fu is expressed in regions that include the acrosome-acroplaxome complex, the perinuclear ring and the manchette, supporting an important role of Fu in sperm head shaping and flagellum protein sorting.

Overexpressed Kif27 is detected in the perinuclear ring of manchette and the head-tail coupling apparatus during spermatogenesis

In prior studies, we showed that Fu interacts with the kinesin Kif27 in cultured cells (Wilson et al., 2009). To explore whether Kif27 could mediate Fu function during spermatogenesis, we generated another transgenic mouse line in which expression of the Kif27-GFP fusion protein was under the control of the *Vasa* promoter (denoted *Vasa-Kif27GFP*). We found that Kif27GFP was expressed in the cytoplasm of all germ cells (Fig. 4C', G') in a pattern similar to FuGFP (supplementary material Fig. S4). Close examination of dry-down or squashed spermatids revealed specific localization of Kif27GFP to the perinuclear ring of the manchette and some weak signal in the manchette in early and elongating spermatids (Fig. 4D', E', H', I'). After the manchette was dismantled, Kif27GFP was detected in the head-tail coupling apparatus (HTCA) where the flagellum connects to the sperm head (Fig. 4F', J'). The distribution of Kif27GFP in elongating spermatids is reminiscent of other manchette transport proteins such as p150Glued (in dynactin) and Hook1 (Kierszenbaum et al., 2011a). Some Kif27GFP signal remained in the residual bodies or droplets but eventually disappeared in mature sperm (Fig. 4F', J'). These findings suggest a possible role of Kif27 in manchette-related functions in head shaping and protein sorting. They also support the notion that Fu and Kif27 function in the same process to mediate manchette function during sperm development.

Fu physically interacts with the small heat shock protein Odf1 and Kif27

Having uncovered a possible manchette-related role for both Fu and Kif27, we asked whether proteins that affect sperm head shaping and manchette function such as Hook1 and Ube2b physically associate with Fu or Kif27 protein. Neither Fu nor Kif27 bound to Hook1 or the ubiquitin-ligase protein Ube2b when expressed in cultured HEK293T cells (data not shown).

We then tested interactions between Fu and Odf1 (Outer dense fiber 1). This was based on the finding that *Odf1*-deficient male mice are infertile due to decapitation of the sperm head (Yang et al., 2012), one of the several abnormal features in *Vasa-Fu* sperm. Epitope-tagged Fu and Odf1 were expressed in HEK293T cells and the lysates were immunoprecipitated using either anti-FLAG or -Myc antibodies. We showed that Fu-FLAG pulled down Odf1-Myc (Fig. 5A). Conversely, Odf1-FLAG brought down Fu-Myc in a similar assay (Fig. 5B). We also determined the domains in Fu necessary for its interactions with Odf1. Odf1 was found to interact with the N-terminal kinase domain of Fu (FuΔC-FLAG) but not the C-terminal regulatory domain (FuΔN-FLAG) (Fig. 5A). These results raised the intriguing possibility that Odf1 could be a kinase substrate for Fu.

Similarly, we investigated the domains in Fu that are required for its interactions with Kif27, a known interacting partner of Fu (Wilson et al., 2009). Only the regulatory domain of Fu (FuΔN-FLAG) could pull down Myc-tagged Kif27 ($Kif27^{Myc}$) using lysates from 293T cells

(supplementary material Fig. S7). By contrast, both FuΔC-FLAG and FuΔN-FLAG failed to immunoprecipitate Myc-tagged Kif7, a Kif27 ortholog. These results support Fu/Kif27 interactions and their conserved roles in multiple tissues.

Discussion

Our studies on Fu provide key insight into mammalian spermatogenesis, in particular, sperm head shaping and tail construction. Following meiosis, the round haploid spermatocytes undergo a series of dramatic cytoskeletal and nuclear changes to generate elongated mature spermatozoa. The main rearrangements during this process include: (1) establishment of the acrosome/acroplaxome and manchette structures, (2) condensation of the nuclear chromatin and (3) assembly and elongation of the flagellum. While these changes are well documented, the molecular mechanisms that underlie these processes are not fully understood. Analysis of *Fu* expression and *Fu*-deficient sperm reveals essential roles of Fu in development of the sperm head and periaxonemal structure. These studies identify Fu as a new player in spermatogenesis and open up new avenues for a molecular understanding of central processes of sperm development.

Fu function in microtubule-based structures in the sperm head

Removal of *Fu* in sperm results in disorganization of the acrosome-acroplaxome complex and the manchette and a misshaped sperm head. This suggests that Fu plays a central role in mediating manchette function. Consistent with this, Fu is detected in the perinuclear ring and the microtubules of the manchette in addition to its expression in the acrosome-acroplaxome domain covering the apical end of the nucleus. The molecular mechanisms by which Fu controls these processes are unknown. A more thorough and high-resolution EM analysis of the acrosome-acroplaxome-nuclear envelope complex may reveal which substructure(s) is affected in *Fu* mutant spermatids. This could facilitate future investigations to uncover the molecular mechanisms by which Fu controls spermatid head shaping.

It is interesting to note that Fu belongs to an ancient family of conserved proteins, most of which execute their functions in association with microtubules. For instance, the *Fu* homolog in the flowering plant *Arabidopsis*, Two-In-One (TIO), localizes to the phragmoplast midzone where the plus end of microtubules are located during plant cytokinesis. TIO was shown to regulate phragmoplast expansion (Oh et al., 2012; Oh et al., 2005). In addition, Tsunami, the *Dictyostelium* homolog of Fu, controls chemotaxis through microtubule interactions (Tang et al., 2008). It is possible that Fu contains a conserved function that is mediated through its interactions with microtubules or specific isoforms of tubulins that are post-translationally modified (Janke and Bulinski, 2011).

The manchette has been proposed to be a major transportation center for proteins destined for the flagellum and Fu may play a role in microtubule organization or cargo transport along the manchette. This could account for the periaxonemal defects in the *Fu* mutant sperm flagellum. However, we cannot rule out the possibility that other mechanisms such as diffusion or selective association are responsible for the observed defects in *Fu* mutants. Abnormal manchette structure has been observed in several knockout mice such as those deficient in Hook1 (Mendoza-Lujambio et al., 2002), a microtubule- and cargo-tethering protein (Maldonado-Baez et al., 2013), Rimbp3, which interacts with Hook1 (Zhou et al., 2009), and Ift88 in the IFT B complex (Kierszenbaum et al., 2011b). Whether these components physically or functionally interact with Fu needs to be further investigated.

While it is clear that *Fu* mutant spermatozoa derived from the epididymis are often decapitated, EM images of spermatids from the testes do not reveal severance of the

connecting region. It is likely that structural weakness in the connecting region becomes apparent only when the flagellum initiates beating. In this scenario, head-tail detachment occurs when mature spermatozoa are released from the epididymis. However, we cannot rule out the possibility that subtle structural defects in the connecting region fail to be detected by EM at the resolution we had.

Fu and Kif27 distribution and function in the perinuclear ring/manchete

The kinesin Kif27 interacts with Fu *in vitro* (Wilson et al., 2009). Overexpressed Kif27 localizes to the perinuclear ring of the manchette and over time translocates to the head-tail coupling apparatus (HTCA) in the neck region of the sperm. Whether Kif27-GFP recapitulates endogenous Kif27 distribution would require additional experimentation using Kif27 antibodies and *Kif27*-deficient mice. Nevertheless, since Fu also resides in the perinuclear ring, this raises the possibility that Fu/Kif27 interactions regulate the transport of specific cargos (perhaps within the manchette) such as accessory components of the sperm flagellum. Identifying Fu substrates and interacting proteins and cargos carried by Kif27 will be a critical step toward understanding the molecular mechanisms by which Fu and Kif27 control sperm development. This would rely on future biochemical studies.

Intramanchette transport (IMT) is one of several models proposed to explain how cytoplasmic spermatid proteins could be sorted to their destination during spermiogenesis (Kierszenbaum, 2002). It is based on the finding that various components of the intraflagellar transport system are found in close association with the microtubule-based manchette. Interestingly, the subcellular distribution of several cargo trafficking proteins in IMT is similar to that of Kif27 during spermiogenesis. For example, both p150Glued (in dynactin) and Hook1, known to participate in vesicle cargo transport in the cytoplasm, move sequentially from the acroplaxome to the manchette and later into the HTCA once the manchette disintegrates (Kierszenbaum et al., 2011b). This is reminiscent of several features of Kif27 distributions. We speculate that Fu/Kif27 could function in conjunction with IMT components in cargo transport to specific destinations.

Fu regulation of the spatial distribution of the accessory structures in the sperm flagellum

We previously reported that Fu is required for the construction or maintenance of the central pair apparatus in the axoneme of motile cilia (Wilson et al., 2009). Unexpectedly, while a large fraction of *Fu*-deficient sperm are immotile, this is not due to central pair defects and instead is a consequence of defective fibrous sheath development. This is even more surprising considering that the fibrous sheath contains periaxonemal structures not present in motile cilia. It is still possible that ultrastructural defects in the central pair apparatus exist in *Vasa-Fu* sperm but are beyond the detection limits of current technology or available tools. Nevertheless, the multiple structural defects in *Fu*-deficient sperm suggest that Fu has additional substrates that are involved in processes other than central pair construction.

The periaxonemal structures include the outer dense fibers and the fibrous sheath (two longitudinal columns and transverse ribs). In *Vasa-Fu* flagella, the fibrous sheath is often distorted and fragmented. Furthermore, at least one additional column is present at a random location around the axoneme. How the loss of Fu compromises the integrity of the fibrous sheath and perturbs normal organization of the longitudinal columns is unknown. The tail defect could result from disrupted Fu functions either in the manchette or other essential processes or in subsequent steps of periaxonemal assembly. Whether Kif27 participates in this process in conjunction with Fu requires additional studies.

Mouse knockouts that disrupt normal organization of the longitudinal columns have been reported. For instance, in mice lacking *Ube2b*, in addition to nuclear anomalies, both

longitudinal columns are present but no longer occupy the normal “8” and “3” positions around the axoneme (Escalier, 2003). This suggests that multiple players are involved in controlling the number and position of the longitudinal columns. Again, identifying Fu substrates and interacting proteins required for the assembly of periaxonemal structure will be a key step toward understanding how Fu controls flagellar development and function.

In human cases of infertility due to sperm motility defects, fibrous sheath defects are often observed in a heterogeneous syndrome called dysplasia of the fibrous sheath (DFS). Abnormal positioning of the longitudinal columns can sometimes be detected in DFS (Chemes and Rawe, 2010). Moreover, a number of genes have been identified in the human DFS syndrome including *Akap3* and *Akap*4 that encode fibrous sheath proteins (Baccetti et al., 2005; Turner et al., 2001). These studies thus provide candidates that function in the same pathway as Fu in controlling fibrous sheath development.

Interactions between Fu and major components of the outer dense fibers

Similar to the fibrous sheath, the outer dense fibers have been implicated not only in conferring structural properties but also playing a regulatory role in flagellar motility. A major component of the outer dense fibers is Odf1. *Odf1* knockout mice exhibit disorganized outer dense fibers, tail detachment and male infertility (Yang et al., 2012), highlighting an essential role of outer dense fibers in proper sperm function. Interestingly, the serine-threonine kinase Cdk5/p35 phosphorylates Odf1 and enhances Odf1 binding to Oip1 (Rnf38), a putative E3 ubiquitin ligase in the sperm tail (Rosales et al., 2004; Rosales et al., 2007). Bearing in mind the caveat of protein overexpression, our finding that Odf1 binds to the Fu kinase domain raises the possibility that Odf1 is a Fu substrate. This also argues that Fu has multiple substrates that function in various structures including the manchette, the outer dense fibers and the fibrous sheath. Functional interactions may also exist between these structures. The challenge is to uncover the molecular mechanisms by which Fu orchestrates the diverse cellular processes during spermiogenesis.

Supplementary Material

Refer to Web version on PubMed Central for supplementary material.

Acknowledgments

We thank Sarah Kaufman, Kurt Thorn, Miao-Hsueh Chen and Jehn-Hsiahn Yang for technical assistance and members of the Chuang laboratory for discussion. Some data for this study were acquired at the Nikon Imaging Center at UCSF/QB3 and CVRI. This work was supported by grants from the National Institutes of Health [R01 HL091915].

References

Ausubel, FM.; Brent, R.; Kingston, RE.; Moore, DD.; Seidman, JG.; Smith, JA.; Struhl, K. Current Protocols in Molecular Biology. Wiley; 2003.

Baccetti B, Collodel G, Estenoz M, Manca D, Moretti E, Piomboni P. Gene deletions in an infertile man with sperm fibrous sheath dysplasia. Hum Reprod. 2005; 20:2790–2794. [PubMed: 15980003]

Chemes HE, Rawe VY. The making of abnormal spermatozoa: cellular and molecular mechanisms underlying pathological spermiogenesis. Cell and tissue research. 2010; 341:349–357. [PubMed: 20596874]

Chen MH, Gao N, Kawakami T, Chuang P-T. Mice deficient in the fused homolog do not exhibit phenotypes indicative of perturbed hedgehog signaling during embryonic development. Mol Cell Biol. 2005; 25:7042–7053. [PubMed: 16055716]

Eddy EM, Toshimori K, O'Brien DA. Fibrous sheath of mammalian spermatozoa. Microscopy research and technique. 2003; 61:103–115. [PubMed: 12672126]

Escalier D. New insights into the assembly of the periaxonemal structures in mammalian spermatozoa. Biology of reproduction. 2003; 69:373–378. [PubMed: 12672659]

Fraser LR. Sperm capacitation and the acrosome reaction. Hum Reprod. 1998; 13(Suppl 1):9–19. [PubMed: 9663766]

Gallardo T, Shirley L, John GB, Castrillon DH. Generation of a germ cell-specific mouse transgenic Cre line, Vasa-Cre. Genesis. 2007; 45:413–417. [PubMed: 17551945]

Greenbaum MP, Iwamori T, Buchold GM, Matzuk MM. Germ cell intercellular bridges. Cold Spring Harbor perspectives in biology. 2011; 3:a005850. [PubMed: 21669984]

Greenbaum MP, Yan W, Wu MH, Lin YN, Agno JE, Sharma M, Braun RE, Rajkovic A, Matzuk MM. TEX14 is essential for intercellular bridges and fertility in male mice. Proceedings of the National Academy of Sciences of the United States of America. 2006; 103:4982–4987. [PubMed: 16549803]

Inaba K. Sperm flagella: comparative and phylogenetic perspectives of protein components. Molecular human reproduction. 2011; 17:524–538. [PubMed: 21586547]

Jan SZ, Hamer G, Repping S, de Rooij DG, van Pelt AM, Vormer TL. Molecular control of rodent spermatogenesis. Biochimica et biophysica acta. 2012; 1822:1838–1850. [PubMed: 22366765]

Janke C, Bulinski JC. Post-translational regulation of the microtubule cytoskeleton: mechanisms and functions. Nature reviews. Molecular cell biology. 2011; 12:773–786.

Kierszenbaum AL. Intramanchette transport (IMT): managing the making of the spermatid head, centrosome, and tail. Molecular reproduction and development. 2002; 63:1–4. [PubMed: 12211054]

Kierszenbaum AL, Rivkin E, Tres LL. Acroplaxome, an F-actin-keratin-containing plate, anchors the acrosome to the nucleus during shaping of the spermatid head. Molecular biology of the cell. 2003; 14:4628–4640. [PubMed: 14551252]

Kierszenbaum AL, Rivkin E, Tres LL. Cytoskeletal track selection during cargo transport in spermatids is relevant to male fertility. Spermatogenesis. 2011a; 1:221–230. [PubMed: 22319670]

Kierszenbaum AL, Rivkin E, Tres LL, Yoder BK, Haycraft CJ, Bornens M, Rios RM. GMAP210 and IFT88 are present in the spermatid golgi apparatus and participate in the development of the acrosome-acroplaxome complex, head-tail coupling apparatus and tail. Developmental dynamics : an official publication of the American Association of Anatomists. 2011b; 240:723–736. [PubMed: 21337470]

Kierszenbaum AL, Tres LL. The acrosome-acroplaxome-manchette complex and the shaping of the spermatid head. Archives of histology and cytology. 2004; 67:271–284. [PubMed: 15700535]

Lo JC, Jamsai D, O'Connor AE, Borg C, Clark BJ, Whisstock JC, Field MC, Adams V, Ishikawa T, Aitken RJ, Whittle B, Goodnow CC, Ormandy CJ, O'Bryan MK. RAB-like 2 has an essential role in male fertility, sperm intra-flagellar transport, and tail assembly. PLoS genetics. 2012; 8:e1002969. [PubMed: 23055941]

Luconi M, Torcia S, Grillo D, Fiorenza MT, Forti G, Mangia F, Baldi E. Enhancement of mouse sperm motility by the PI3-kinase inhibitor LY294002 does not result in toxic effects on preimplantation embryo development. Hum Reprod. 2005; 20:3500–3504. [PubMed: 16126754]

Maldonado-Baez L, Cole NB, Kramer H, Donaldson JG. Microtubule-dependent endosomal sorting of clathrin-independent cargo by Hook1. The Journal of cell biology. 2013; 201:233–247. [PubMed: 23589492]

Mendoza-Lujambio I, Burfeind P, Dixkens C, Meinhardt A, Hoyer-Fender S, Engel W, Neesen J. The Hook1 gene is non-functional in the abnormal spermatozoon head shape (azh) mutant mouse. Human molecular genetics. 2002; 11:1647–1658. [PubMed: 12075009]

Moreno RD, Palomino J, Schatten G. Assembly of spermatid acrosome depends on microtubule organization during mammalian spermiogenesis. Developmental biology. 2006; 293:218–227. [PubMed: 16540102]

Nagy, A.; Gertsenstein, M.; Vintersten, K.; Behringer, R. Manipulating the Mouse Embryo: A Laboratory Manual. Third Edition. Cold Spring Harbor, NY: Cold Spring Harbor Laboratory Press; 2003.

Nozawa YI, Yao E, Lin C, Yang JH, Wilson CW, Gacayan R, Chuang PT. Fused (Stk36) is a ciliary protein required for central pair assembly and motile cilia orientation in the mammalian oviduct.

Developmental dynamics : an official publication of the American Association of Anatomists. 2013; 242:1307–1319. [PubMed: 23907739]

O'Donnell L, Nicholls PK, O'Bryan MK, McLachlan RI, Stanton PG. Spermiation: The process of sperm release. Spermatogenesis. 2011; 1:14–35. [PubMed: 21866274]

Oh SA, Allen T, Kim GJ, Sidorova A, Borg M, Park SK, Twell D. Arabidopsis Fused kinase and the Kinesin-12 subfamily constitute a signalling module required for phragmoplast expansion. The Plant journal : for cell and molecular biology. 2012; 72:308–319. [PubMed: 22709276]

Oh SA, Johnson A, Smertenko A, Rahman D, Park SK, Hussey PJ, Twell D. A divergent cellular role for the FUSED kinase family in the plant-specific cytokinetic phragmoplast. Current biology : CB. 2005; 15:2107–2111. [PubMed: 16332535]

Oko R, Clermont Y. Light microscopic immunocytochemical study of fibrous sheath and outer dense fiber formation in the rat spermatid. The Anatomical record. 1989; 225:46–55. [PubMed: 2476045]

Pazour GJ, Dickert BL, Vucica Y, Seeley ES, Rosenbaum JL, Witman GB, Cole DG. Chlamydomonas IFT88 and its mouse homologue, polycystic kidney disease gene tg737, are required for assembly of cilia and flagella. The Journal of cell biology. 2000; 151:709–718. [PubMed: 11062270]

Quinn P, Kerin JF, Warnes GM. Improved pregnancy rate in human in vitro fertilization with the use of a medium based on the composition of human tubal fluid. Fertility and sterility. 1985; 44:493–498. [PubMed: 3902512]

Rosales JL, Lee BC, Modarressi M, Sarker KP, Lee KY, Jeong YG, Oko R, Lee KY. Outer dense fibers serve as a functional target for Cdk5.p35 in the developing sperm tail. The Journal of biological chemistry. 2004; 279:1224–1232. [PubMed: 14581463]

Rosales JL, Sarker K, Ho N, Broniewska M, Wong P, Cheng M, van der Hoorn FA, Lee KY. ODF1 phosphorylation by Cdk5/p35 enhances ODF1-OIP1 interaction. Cellular physiology and biochemistry : international journal of experimental cellular physiology, biochemistry, and pharmacology. 2007; 20:311–318.

Sambrook, J.; Russell, DW. Molecular Cloning: A Laboratory Manual. Cold Spring Harbor, NY: Cold Spring Harbor Laboratory Press; 2001.

Sironen A, Hansen J, Thomsen B, Andersson M, Vilkki J, Toppari J, Kotaja N. Expression of SPEF2 during mouse spermatogenesis and identification of IFT20 as an interacting protein. Biology of reproduction. 2010; 82:580–590. [PubMed: 19889948]

Soriano P. Generalized lacZ expression with the ROSA26 Cre reporter strain. Nat Genet. 1999; 21:70–71. [PubMed: 9916792]

Sperry AO. The dynamic cytoskeleton of the developing male germ cell. Biology of the cell / under the auspices of the European Cell Biology Organization. 2012; 104:297–305. [PubMed: 22276751]

Suarez SS. Control of hyperactivation in sperm. Human reproduction update. 2008; 14:647–657. [PubMed: 18653675]

Tang L, Franca-Koh J, Xiong Y, Chen MY, Long Y, Bickford RM, Knecht DA, Iglesias PA, Devreotes PN. tsunami, the Dictyostelium homolog of the Fused kinase, is required for polarization and chemotaxis. Genes & development. 2008; 22:2278–2290. [PubMed: 18708585]

Tarulli GA, Stanton PG, Meachem SJ. Is the adult Sertoli cell terminally differentiated? Biology of reproduction. 2012; 87:13–11. 11. [PubMed: 22492971]

Turner RM, Musse MP, Mandal A, Klotz K, Jayes FC, Herr JC, Gerton GL, Moss SB, Chemes HE. Molecular genetic analysis of two human sperm fibrous sheath proteins, AKAP4 and AKAP3, in men with dysplasia of the fibrous sheath. Journal of andrology. 2001; 22:302–315. [PubMed: 11229805]

Wilkinson DG, Nieto MA. Detection of messenger RNA by in situ hybridization to tissue sections and whole mounts. Methods Enzymol. 1993; 225:361–373. [PubMed: 8231863]

Wilson CW, Nguyen CT, Chen MH, Yang JH, Gacayan R, Huang J, Chen JN, Chuang PT. Fused has evolved divergent roles in vertebrate Hedgehog signalling and motile ciliogenesis. Nature. 2009; 459:98–102. [PubMed: 19305393]

Yang K, Meinhardt A, Zhang B, Grzmil P, Adham IM, Hoyer-Fender S. The small heat shock protein ODF1/HSPB10 is essential for tight linkage of sperm head to tail and male fertility in mice. Mol Cell Biol. 2012; 32:216–225. [PubMed: 22037768]

Zhang Q, Nishimura D, Vogel T, Shao J, Swiderski R, Yin T, Searby C, Carter CS, Kim G, Bugge K, Stone EM, Sheffield VC. BBS7 is required for BBSome formation and its absence in mice results in Bardet-Biedl syndrome phenotypes and selective abnormalities in membrane protein trafficking. Journal of cell science. 2013; 126:2372–2380. [PubMed: 23572516]

Zhou J, Du YR, Qin WH, Hu YG, Huang YN, Bao L, Han D, Mansouri A, Xu GL. RIM-BP3 is a manchette-associated protein essential for spermiogenesis. Development. 2009; 136:373–382. [PubMed: 19091768]

- Fused (Fu)-deficient male mice are infertile
- Fu is required for mammalian sperm head development
- Fu controls proper organization of the periaxonemal structure in the flagellum
- Fu localizes to multiple microtubule-organizing structures during spermatogenesis
- Fu interacts with the outer dense fiber protein Odf1 and kinesin Kif27

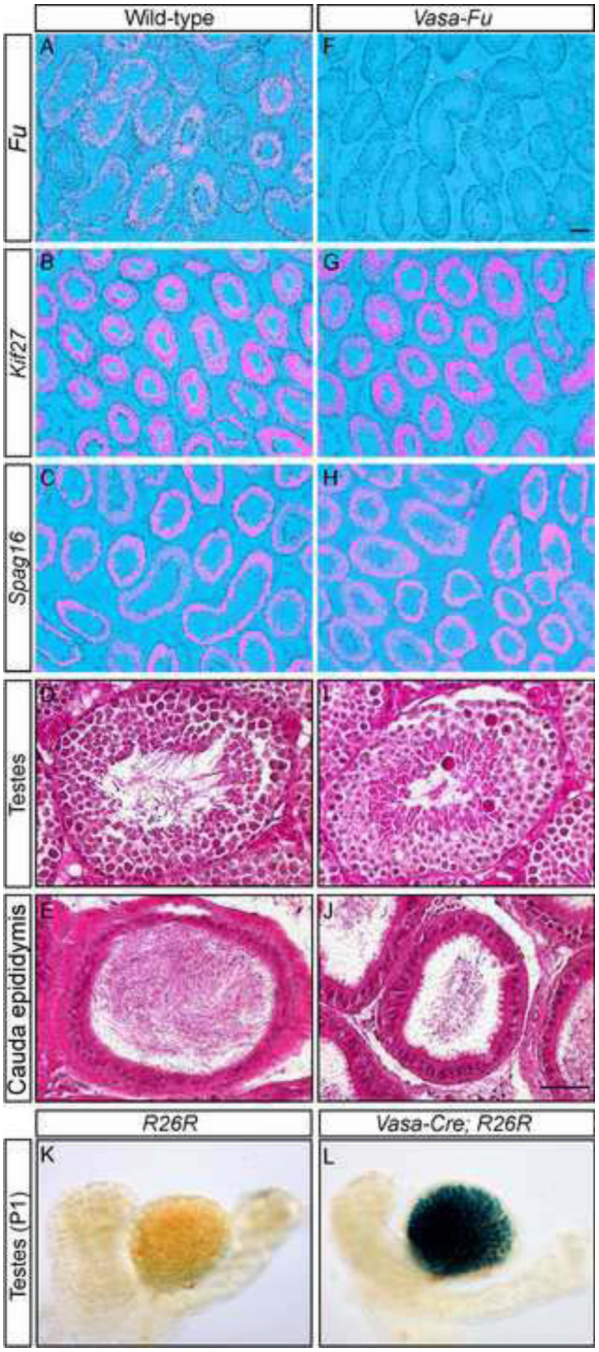

Figure 1. Conditional deletion of *Fused* in the germ cells leads to reduced sperm count despite normal morphology of testes and epididymides

(A–C, F–H) Isotopic *in situ* hybridization using ^{33P}-UTP-labeled riboprobes (pink) derived from *Fu*, *Kif27*, *Spag16* on paraffin sections of wild-type (A–C) and *Vasa-Fu* (F–H) mouse adult testes. *Fu*, *Kif27*, *Spag16* were all expressed in the germ cells residing in the seminiferous tubules. *Vasa-Fu* testes in which Vasa-Cre converted a conditional allele of *Fu* into a null allele showed no *Fu* expression (F). *Kif27* and *Spag16* expressions in the testes were unaltered in the absence of *Fu*. (D, E, I, J) Hematoxylin and eosin-stained sections of testes (D, I) and cauda epididymis (E, J) from wild-type and *Vasa-Fu* adult mice. The seminiferous tubules appeared morphologically normal in the absence of *Fu* and were

populated by germ cells and Sertoli nurse cells. *Fu*-deficient cauda epididymis where mature spermatozoa are stored was also morphologically normal. However, a decrease in spermatozoa density was detected in cauda epididymides of *Vasa-Fu* mice. Scale bar = 100 μm for A–C and F–H; 50 μm for D, E, I, J. (K, L) Whole-mount β-gal (LacZ) staining of testes and epididymides from *R26R* and *Vasa-Cre; R26R* mice at postnatal (p) day 1. Specific β-gal staining was observed in the developing seminiferous tubules of the *Vasa-Cre; R26R* testes in which Cre expression activated a β-gal reporter from the *R26R* locus.

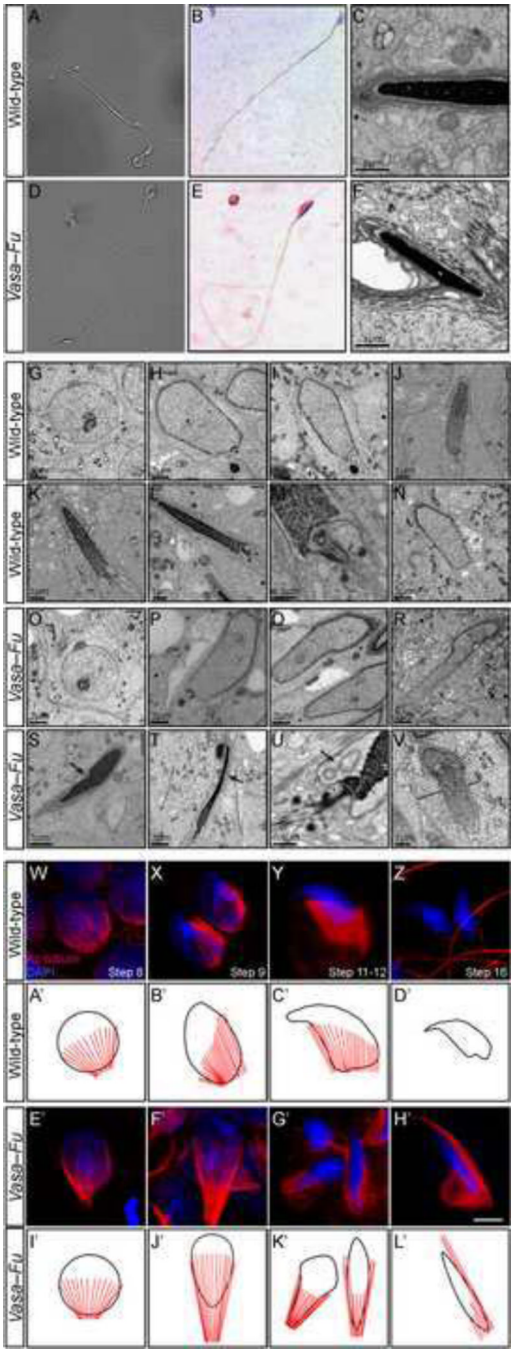

Figure 2. *Vasa-Fu* spermatozoa have disrupted head morphology associated with perturbed manchette formation and function

(A, D) Phase contrast images of mature spermatozoa derived from the cauda epididymis of wild-type and *Vasa-Fu* adult mice. *Vasa-Fu* flagella were of normal length and contained all the main structures (head, midpiece and flagellum). (B, E) Hematoxylin and eosin-stained spermatozoa derived from the cauda epididymis of wild-type and *Vasa-Fu* adult mice. The nucleus stained blue. The *Vasa-Fu* sperm head was elongated and lacked the characteristic hook shape in wild-type mouse spermatozoa heads. (C, F) Transmission electron micrographs of wild-type and *Vasa-Fu* mature spermatozoa from the testes. Wild-type sperm heads (C) showed a tight association between the nucleus (Nu) (black, electron-

dense) and the acrosome cap (Ac) (dark grey). By contrast, the sperm head from *Vasa-Fu* (F) had a large gap between the nucleus and the acrosome cap. (G–V) Transmission electron micrographs of wild-type and *Vasa-Fu* spermatids. (G, O) Cap phase spermatid (steps 4–7). The round spermatids are characterized by the establishment of the acrosome/acroplaxome complex at one end of the nucleus. (H–J, P–R) Acrosome phase spermatids (steps 8–14). The manchette was discerned by microtubules on either side of the nucleus. Alteration in the nuclear shape, gaps in the acrosome/acroplaxome complex and excessive elongation of the manchette were observed in elongating *Vasa-Fu* spermatids. (K, L, S, T) Maturation phase spermatids (steps 15–19). The nucleus was fully condensed and elongated. The annulus (two large dots) began to migrate to form the midpiece. In *Vasa-Fu* spermatids, the nucleus and the perinuclear ring were distorted (S) (arrow). Thinning of the extended nucleus and fragmentation of the membranes could also be seen (T) (arrow). (M, U) High-resolution view of the connecting piece in an elongating spermatid. Note the large vesicles (arrow) at the base of the nucleus in the *Vasa-Fu* spermatid (U). (N, V) High-resolution view of the manchette microtubules in wild-type and *Vasa-Fu* spermatids. The microtubules appeared more abundant and were also disordered and asymmetrical in the mutants (compare black lines in V to N). (W–Z) Immunostaining of wild-type germ cells derived from the testes at various stages of spermiogenesis (steps 8–16 shown). The manchette was marked by anti-acetylated (Ac) tubulin antibodies (red) while the nucleus was stained with DAPI (blue). The flagellum was also labeled by Ac-tubulin (Z). (E'–H') Immunostaining of *Vasa-Fu* germ cells derived from the testes at similar stages. The manchette structure appeared around the nucleus (E') but became disorganized subsequently throughout spermiogenesis (F'–H'). Ectopic microtubules and defective nuclear head shaping were noticeable (F'–H'). Scale bar = 5 μm for W–Z, E'–H'. (A'–D', I'–L') Schematic representation of manchette (red) development in relation to the nucleus (black) during spermiogenesis in wild-type and *Vasa-Fu* spermatids. In *Vasa-Fu* mutant spermatids, the manchette is abnormally elongated and also present ectopically and the nucleus is misshapen.

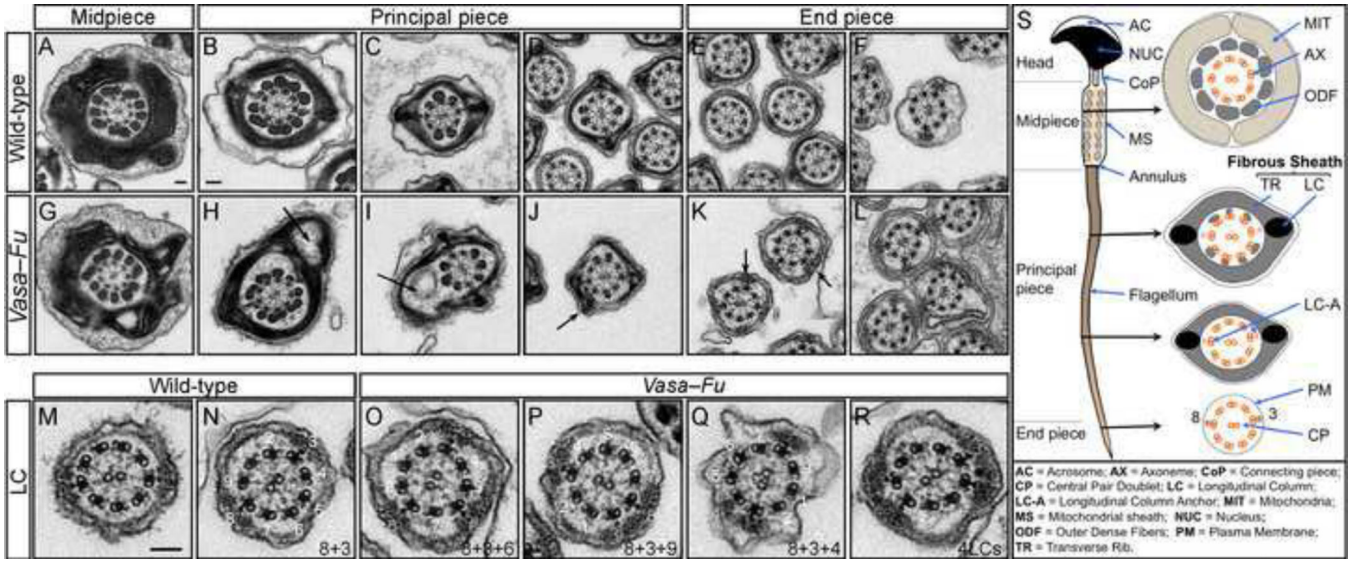

Figure 3. Testicular *Vasa-Fu* sperm flagella display periaxonemal abnormalities

(A–L) Transmission electron micrographs of sperm from wild-type and *Vasa-Fu* adult mouse testes. Cross sections through the midpiece, principal piece and end piece were shown. In the principal piece, large gaps and vesicles (arrows in H, I) were observed in the transverse ribs of the fibrous sheath with unidentified material within. In more distal sections, an additional longitudinal column (LC) (arrows in J, K) that surrounds the axoneme was detected. The LCs are characterized by electron-dense material anchored to a microtubule doublet of the axoneme. Scale bar = 0.1 μm for A, G. Scale bar = 0.1 μm for B–F, H–L. (M–R) Distribution of longitudinal columns in wild-type and *Vasa-Fu* flagella derived from the testes. The numbers (1–9) refer to the position of microtubule doublets; the LCs surround microtubule doublets at positions 8 and 3 in wild-type sperm (also see S). An extra LC was detected at position 6 in (O), 9 in (P) and 4 in (Q). Approximately 5% of axonemes examined had two additional longitudinal columns (R). Scale bar = 0.1 μm for M–R. (S) Schematic diagram of mouse sperm. The head is connected to the flagellum by a connecting piece, from which nine outer dense fibers (ODFs) originate from the head-tail coupling apparatus (HTCA) and extend into the flagellum. The flagellum is characterized by a “9+2” motile axoneme in which nine microtubule doublets surround a central pair. The doublets are numbered clockwise starting with the doublet on the plane that bisects the central pair. Each ODF surrounds a microtubule doublet in the midpiece. The principal piece is covered by the fibrous sheath (FS) that contains two longitudinal columns, each replacing an ODF (at microtubule doublet positions 8 and 3). The longitudinal columns are associated with a specific microtubule doublet through a longitudinal anchor (LC-A). The columns are connected by keratinous transverse ribs and are proposed to maintain the structural integrity of the flagellum and affect the plane of flagellar motion and the waveform of the beat. The periaxonemal structures provide stability and strength to the flagellum.

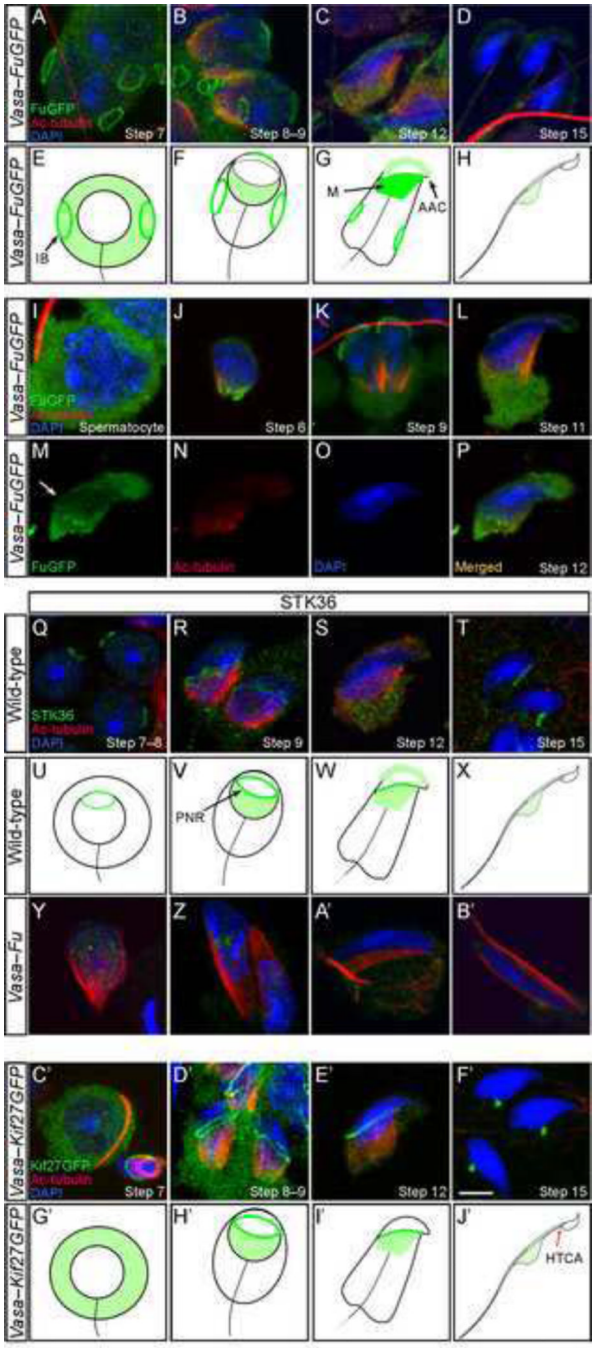

Figure 4. FuGFP and Kif27GFP localize to various microtubule-organizing centers of the developing sperm

(A–D, I–P) Confocal immunofluorescence of testicular cells derived from *Vasa-FuGFP* transgenic mice where a *Fu-GFP* fusion protein was expressed under the germ cell-specific *Vasa* promoter. Cells were stained with antibodies against GFP (green) and acetylated tubulin (red) while the nucleus was stained with DAPI (blue). FuGFP was seen in the intercellular bridges (A) on the plasma membrane of round spermatids. The signal in the intercellular bridges persisted through the elongation steps of spermiogenesis. In spermatids with condensing chromatin (B, C), FuGFP was found in the manchette, the perinuclear ring and the acrosome-acroplaxome. In elongated spermatids (D), the manchette disappeared and

the FuGFP signal was reduced. (E–H) Schematic diagram illustrating the localization of FuGFP (green) during spermiogenesis. (I–L) Additional stages of *Vasa-FuGFP* during spermiogenesis. Spermatocytes had broad cytoplasmic FuGFP staining (I). FuGFP staining was present in the manchette of a round spermatid (J) and in the developing acrosome-acroplaxome (J–L). (M–P) A step 12/13 elongating *Vasa-FuGFP* spermatid displayed immunofluorescence in the acrosome-acroplaxome, perinuclear ring (arrow) and manchette. (Q–T) Confocal immunofluorescence of testicular cells derived from wild-type adult mice. Cells were stained with antibodies against STK36 (green) and acetylated (Ac) tubulin (red); the nucleus was stained with DAPI (blue). STK36 signal was primarily detected in the perinuclear ring of round (Q), elongating (R, S) and elongated (T) spermatids. Weaker STK36 staining was also present in the manchette and the acrosome-acroplaxome (S). (U–X) Schematic diagram illustrating the localization of endogenous Fu (Stk36) during spermiogenesis. Not drawn to scale. (Y–B') Confocal immunofluorescence of testicular cells derived from *Vasa-Fu* adult mice. STK36 staining was residual and non-specific. (C'–F') Confocal immunofluorescence of testicular cells derived from *Vasa-Kif27GFP* transgenic mice. GFP signal was detected in the cytoplasm of round spermatids (C'). In elongating spermatids (D', E'), specific signal was detected in the manchette and along the perinuclear ring that borders it. Kif27GFP signal translocated to the head-tail coupling apparatus (HTCA) at later stages (F'). After spermiation, no GFP signal was detected in the spermatozoa for either FuGFP or Kif27GFP. Scale = 5 μm for A–D, I–T, Y–B'. (G'–J') Schematic diagram illustrating the localization of Kif27GFP (green) during spermiogenesis. Not drawn to scale. IB, intercellular bridge; M, manchette; AAC, acrosome-acroplaxome complex, PNC, perinuclear ring, HTCA, head-tail coupling apparatus.

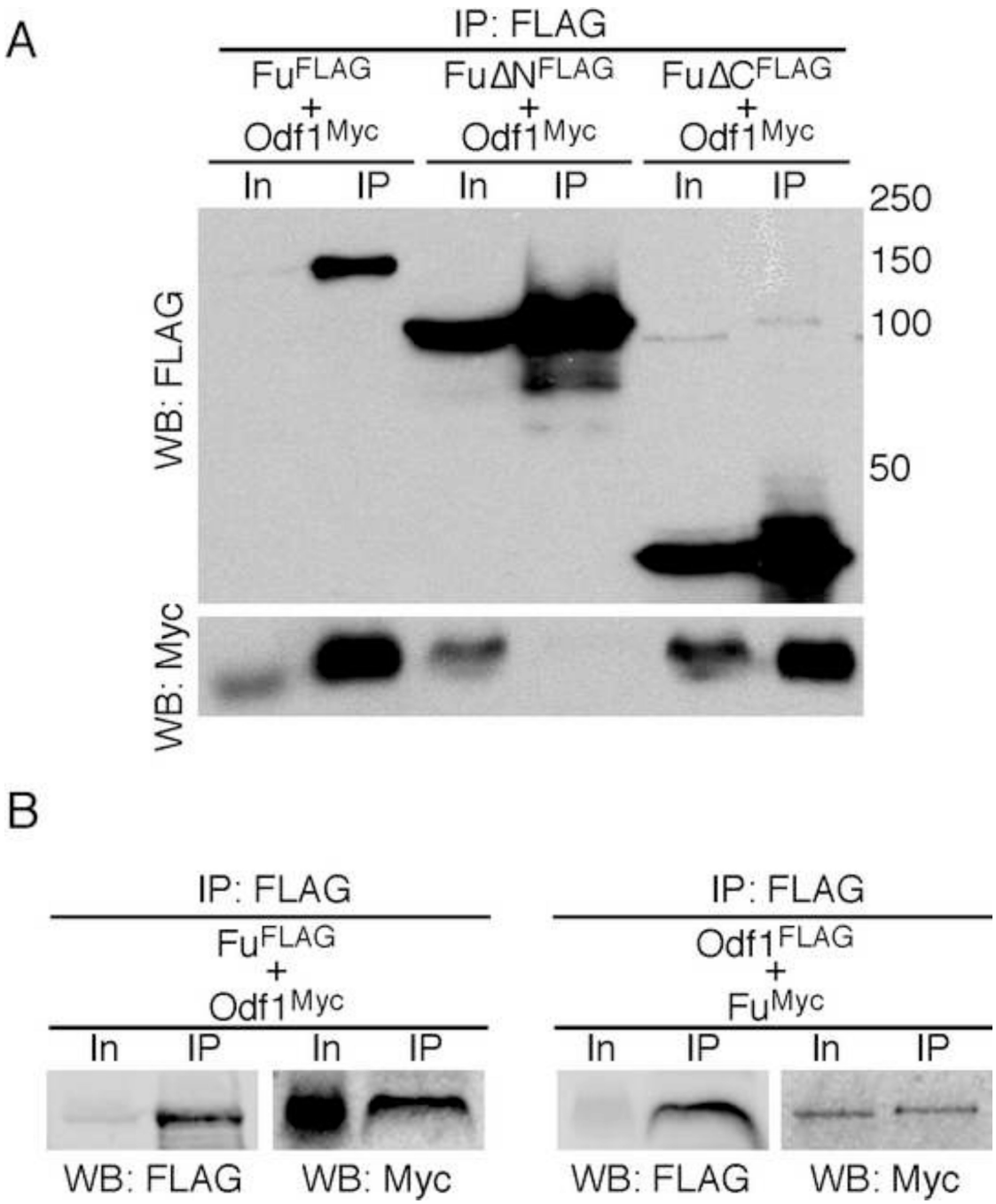

Figure 5. Fu interacts with the heat-shock family protein Odf1

(A) Western blot of immunoprecipitated Fu^{FLAG} and deletion mutants of Fu ($FuΔN^{FLAG}$ and $FuΔC^{FLAG}$) to test physical interactions between Fu and Odf1 using HEK293T cell lysates. $Odf1^{Myc}$ was pulled down from the cell lysate when Fu^{FLAG} or $FuΔC^{FLAG}$ (lacking the C-terminal regulatory domain) was immunoprecipitated. However, $Odf1^{Myc}$ failed to be co-immunoprecipitated with $FuΔN^{FLAG}$ that lacks the kinase domain. (B) Western blot of immunoprecipitated Fu^{FLAG} or $Odf1^{Myc}$ from HEK293T cell lysates to examine their physical interactions. Fu^{Myc} can be pulled down when $Odf1^{FLAG}$ was immunoprecipitated with anti-FLAG agarose. In a control experiment, $Odf1^{FLAG}$ failed to bring down $Sufu^{Myc}$

(not shown). In, input; IP, immunoprecipitation; WB, Western blot. The numbers indicate locations of protein size standards.

Table 1

Phenotypic analysis of wild-type and *Vasa-Fu* male mice

	Testis weight (mg)	Testis sperm count ($\times 10^3$/mg)	Cauda epididymis weight (mg)	Cauda epididymis sperm count ($\times 10^3$/mg)	Fertility (# fertile/total)
Wild-Type (n=6)	95.5±2.2	194.7±10.9	8.7±0.5	1641.4±130.9	3/3
Vasa-Fu (n=5)	96.0±3.9	168.0±5.2*	7.5±0.6*	1149.3±169.6*	0/3

All values are means ± standard error of the mean (s.e.m.).

* $P < 0.05$ compared to wild-type (unpaired Student's *t*-test).

Two testes from each mouse were collected.

Table 2

Wild-type and *Vasa-Fu* mouse sperm phenotypes

	% Immotile (Capacitated)	% Motile Non-Progressive (Capacitated)	% Motile Progressive (Capacitated)	% Motile (Non-capacitated)	%Sperm decapitation (Non-capacitated)	% Periaxonemal defects (Testis)
Wild-Type	20.3±7.6 (*n*=4)	6.4±0.8 (*n*=4)	73.7±6.7 (*n*=4)	49.7±0.9 (*n*=5)	5.8±1.6 (*n*=5)	0.1±0.1 (*n*=3)
Vasa-Fu	51.0±3.0* (*n*=2)	26.4±10.8* (*n*=2)	22.6±7.8* (*n*=2)	30.4±3.9* (*n*=4)	36.8±2.7** (*n*=4)	57.6±6.4* (*n*=3)

All values are means ± standard error of the mean (s.e.m.).

* P < 0.05 compared to wild-type;

** P < 0.001 compared to wild-type (unpaired Student's *t*-test).

Mouse sperm were collected from the cauda epididymis unless otherwise noted.

Only spermatozoa with head and flagellum attached were counted for motility measurements.

Periaxonemal defects of the sperm flagellum were counted in EM micrographs of tissue cross-sections.